Frustrated superconducting junction with tricomponent pairing gap functions

Chao Xu [1,*], Wang Yang,[2,*] and Congjun Wu [3,4,5,6,†]

[1]*Kavli Institute for Theoretical Sciences, University of Chinese Academy of Sciences, Beijing 100190, China*
[2]*School of Physics, Nankai University, Tianjin 300071, China*
[3]*New Cornerstone Science Laboratory, Department of Physics, School of Science, Westlake University, 310024 Hangzhou, China*
[4]*Institute for Theoretical Sciences, WestLake University, Hangzhou 310024, China*
[5]*Key Laboratory for Quantum Materials of Zhejiang Province, School of Science, Westlake University, Hangzhou 310024, China*
[6]*Institute of Natural Sciences, Westlake Institute for Advanced Study, Hangzhou 310024, Zhejiang, China*

We study a superconducting heterojunction with one side characterized by the unconventional chiral p-wave gap function $p_x \pm i p_y$ and the other side the conventional s-wave one. Though a relative phase of $\pm\frac{\pi}{2}$ between any two components of gap functions is favored in the junction region, mutual phase differences cannot achieve $\pm\frac{\pi}{2}$ simultaneously, which results in frustration. Based on a Ginzburg-Landau free-energy analysis, the frustrated pattern is determined to be $s + i\eta_1[\exp(i\eta_2\varphi/2)p_x + \eta_3 \exp(-i\eta_2\varphi/2)p_y]$ with $\eta_j = \pm 1$ ($j = 1, 2, 3$), where φ is the phase difference between the p_x- and p_y-wave gap functions. Furthermore, we find that the junction exhibits an anisotropic magnetoelectric effect, manifesting itself as an anisotropic spin magnetization along the edge of the junction.

I. INTRODUCTION

Chiral superconductors constitute a class of superconducting states of matter characterized by unconventional gap functions, spontaneous time-reversal symmetry breaking, and nontrivial topological properties [1]. The topological structure in the pairing wave functions leads to exotic phenomena, including the emergence of Majorana zero modes in vortex cores [2–6] and chiral Majorana fermions on the boundary of the system [7–9], which can be useful in realizing topological quantum computations [10–14]. The superconducting Sr_2RuO_4 [15–18] and UPt_3 materials [19–22] have been proposed to host chiral superconductivity with p- and f-wave pairing gap functions, respectively, though there are still debates over the pairing nature of these materials [16,23–25] despite intensive theoretical and experimental studies [26–34].

In general, when pairing orders in several channels coexist, the system may develop a superposition of gap function symmetries which spontaneously breaks time-reversal symmetry. A typical pattern of time-reversal symmetry breaking is that a relative $\pm\frac{\pi}{2}$ phase difference develops between two different pairing channels with different symmetries, which has been studied in various systems including the ^{3}He-A superfluid phase [35,36] and superconductors with $p_x + i p_y$ [4,12,37–42] and $d_{x^2-y^2} + i d_{xy}$ [43–57] gap function symmetries. The mixing between the s- and p-wave gap function symmetries with a relative phase difference $\pm\frac{\pi}{2}$ was proposed by Wu and Hirsch [58] in the context of superfluid insta-

bility of dipolar fermions and was later generalized to other systems [59–61]. Mixed gap function symmetries breaking time-reversal symmetry have also been proposed in the iron-based superconductors [62,63] and other related systems, such as $s + id$ [62,64–69] and $s + is$ [63,69–76]. On the other hand, the interplays among three or more different superconducting order parameters remain less explored [77–81].

In this paper, we study the superconductor-superconductor junction with one side characterized by a chiral p-wave gap function symmetry and the other side the conventional s-wave one, respectively, as illustrated in Fig. 1. In the junction region, three gap function symmetries coexist due to the proximity effect. The linear Josephson coupling is not allowed due to their different symmetries, and any two of them can only be coupled via the quadratic Josephson term at the lowest order. Any two of them favor a relative phase of $\pm\frac{\pi}{2}$; however, the system is frustrated since a simultaneous mutual $\pm\frac{\pi}{2}$ phase difference is impossible among three order parameters.

This frustration is different from that of the antiferromagnetism defined in the triangular lattice in which the bilinear Heisenberg coupling is analogous to the linear Josephson coupling. To determine the frustrated pattern of the gap functions, a Ginzburg-Landau (GL) free-energy analysis is performed. The gap function structure in the junction region is solved to exhibit an exotic form $s + i\eta_1[\exp(i\eta_2\varphi/2)p_x + \eta_3 \exp(-i\eta_2\varphi/2)p_y]$, as shown in Fig. 2, where φ is the phase difference between the p_x- and p_y-pairing order parameters, and $\eta_j = \pm 1$ ($j = 1, 2, 3$). By fixing the chirality deep in the p-wave layer as the boundary condition, the time-reversal and reflection symmetries are explicitly broken. The frustration spontaneously breaks the C_4 symmetry and can be viewed as a frustration-induced nematic superconductivity. In the junction
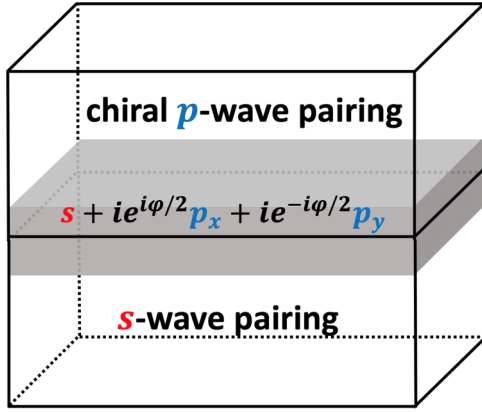
FIG. 1. The heterojunction formed by a chiral p-wave superconductor in the upper space and an s-wave superconductor in the lower space. A mixed tricomponent gap function develops near the interface of the heterojunction induced by the proximity effect. The z direction is chosen along the crystalline c axis as pointing upwards.

region, the tricomponent pairing further breaks the residual C_4 symmetry, and the four degenerate configurations satisfy $\eta_2\eta_3 = -\eta_c$ ($\eta_c = \pm1$) when the boundary condition is chosen as $p_x + i\eta_c p_y$.

Furthermore, we find that the system exhibits an anisotropic magnetoelectric effect around the edge of the junction, consistent with the C_4 symmetry breaking. The magnetoelectric effect also manifests itself as the emergence of an anisotropic spin magnetization on the edge of the junction, which can be analyzed through the splitting of the two spin-polarized chiral Majorana edge modes.

The rest of this paper is organized as follows. In Sec. II, the GL free-energy analysis is performed, and the origin of frustration among gap functions is illustrated. The anisotropic magneto-electric effect and the edge magnetization are studied in Sec. III. The relation between the edge magnetization and the gap function mixing is presented in Sec. IV. Conclusions are presented in Sec. V.
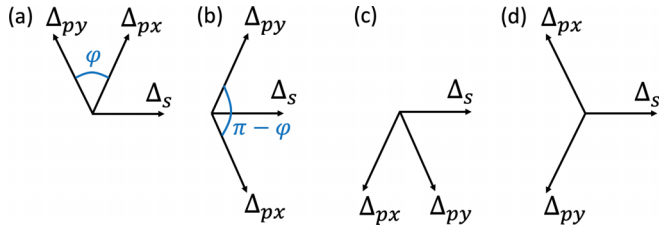

FIG. 2. Plots of the four tricomponent pairing configurations with the positive chirality, i.e., $s + i\eta_1[\exp(i\eta_2\varphi/2)p_x + \eta_3\exp(-i\eta_2\varphi/2)p_y]$, where $\eta_2\eta_3 = -1$. In (a)–(d), $|\Delta_{px}| = |\Delta_{py}|$, and the phase of the s-wave pairing is fixed to be zero. The configurations in (b)–(d) can be obtained by performing C_4 rotations at the angles of $\pi/2$, π, and $3\pi/2$ on the configuration of (a), respectively. We note that the rotations are performed in the orbital space not on the phase configurations of the gap functions illustrated in (a)–(d). Hence, the rotation of $\pi/2$ keeps Δ_s unchanged, and $\Delta_{px} \to \Delta_{py}$ and $\Delta_{py} \to -\Delta_{px}$.

II. GL free-energy analysis

A. Brief review of the $p_x \pm ip_y$ pairing

We first briefly review the GL free-energy analysis for the chiral p-wave superconductor with the $p_x \pm ip_y$ pairing. The point group symmetry is assumed to be the D_{4h} group, which applies to a tetrahedral lattice system. The most general GL free energy respecting the U(1) gauge, the time reversal, and the D_{4h} point group symmetries up to quartic order is

$$f_1 = \alpha_p(|\Delta_{px}|^2 + |\Delta_{py}|^2) - g_{pp}|\Delta_{px}^*\Delta_{py} - \Delta_{py}^*\Delta_{px}|^2$$
$$+ \beta_p(|\Delta_{px}|^2 + |\Delta_{py}|^2)^2 + \beta_p'(|\Delta_{px}|^4 + |\Delta_{py}|^4), \quad (1)$$

in which Δ_{px}, Δ_{py} are the order parameters of the p_x- and p_y-wave pairing gap functions, respectively; $\alpha_p < 0$ in the superconducting state; $\beta_p > 0$ is the coefficient of the corresponding rotationally invariant phase-nonsensitive quartic term; the β_p' term breaks the SO(2) rotational symmetry down to C_4; $g_{pp} > 0$ is the coefficient of the term which contains the quadratic Josephson coupling $(\Delta_{px}^*\Delta_{py})^2 + \text{H.c.}$; and only the uniform parts of the free energy are kept while the gradient terms are neglected.

Since g_{pp} is generically positive, the energy of the quadratic Josephson term is lowered if a $\pm\frac{1}{2}\pi$ phase difference is developed between Δ_{px} and Δ_{py}. As a result, the $p_x \pm ip_y$ pairing is favored which spontaneously breaks time-reversal symmetry. Though the $p_x \pm ip_y$ pairing breaks both U(1) gauge and C_4 rotational symmetries, it is invariant under $GR(\hat{z}, \pi/2)$, where $R(\hat{z}, \pi/2)$ is the $\pi/2$ rotation around the z axis in the orbital space and G is the gauge transformation by $\pm\pi/4$ of the electrons (i.e., $\pm\pi/2$ phase rotation of the Cooper pairs). Here, $L_z + \frac{1}{2}N$ remains a conserved quantity when $\beta_p' = 0$.

Here, we make a comment on the use of Eq. (1), where terms only up to quartic order are kept in the GL free-energy functional. For our purpose, we are mostly interested in the symmetry of the pairing gap function, not its quantitative values. Based on Landau's paradigm, phases are classified by symmetry-breaking patterns, namely, the symmetry-breaking pattern remains the same in the same phase and changes only when phase transitions take place. As a result, the symmetry-breaking pattern determined by the low-order expansion of the GL free energy in the vicinity of T_c is valid in the entire phase even beyond the applicable range of the expansion, which is nicely explained in Chapter 5 of the celebrated textbook in Ref. [82]. The same philosophy is used in later discussions of the superconducting phase with a tricomponent pairing gap function.

B. Minimization of the free energy for the junction

Next, we proceed to discuss the tricomponent pairing gap function as a consequence of the competition among three pairing order parameters. The system under consideration is a heterojunction formed by a chiral p-wave superconductor in the upper space and an s-wave superconductor in the lower space, as shown in Fig. 1. The pairing Hamiltonians deep

inside the upper and lower spaces in Fig. 1 are given by

$$\hat{\Delta}_p = \sum_{\vec{k}\alpha\beta} \frac{1}{k_f}(|\Delta_{px}|k_x + i|\Delta_{py}|k_y)(\sigma^z i\sigma^y)_{\alpha\beta} c^\dagger_{\vec{k}\alpha} c^\dagger_{-\vec{k}\beta},$$

$$\hat{\Delta}_s = |\Delta_s| \sum_{\vec{k}} c^\dagger_{\vec{k}\uparrow} c^\dagger_{-\vec{k}\downarrow}, \tag{2}$$

in which $\alpha, \beta = \uparrow, \downarrow$ are the spin indices, and $c^\dagger_{\vec{k}\alpha}$ is the electron creation operator with momentum $\vec{k}$ and spin α.

On the other hand, due to the proximity effect, there is a mixture of p-wave (Δ_{px}, Δ_{py}) and s-wave (Δ_s) superconducting order parameters in the junction region. To study the pattern of mixing, we take a GL free-energy analysis. Because of the heterostructure, the point group symmetry becomes the planar C_{4v} group, which contains the C_4 rotations and four reflections. Assuming the U(1) gauge, time reversal, and C_{4v} symmetries, the free-energy density up to the quartic order takes the form:

$$f = f_p + f_s + f_{sp} + f'_{sp}, \tag{3}$$

in which

$$f_s = K_s|\nabla_z \Delta_s|^2 + \alpha_s|\Delta_s|^2 + \beta_s|\Delta_s|^4,$$

$$f_p = K_p(|\nabla_z \Delta_{px}|^2 + |\nabla_z \Delta_{py}|^2) + f_1,$$

$$f_{sp} = g_{sp}[\Delta_s^{*2}(\Delta_{px}^2 + \Delta_{py}^2) + \text{c.c.}],$$

$$f'_{sp} = \gamma(|\Delta_{px}|^2 + |\Delta_{py}|^2)|\Delta_s|^2, \tag{4}$$

where f_1 within f_p is given by Eq. (1) and c.c. is complex conjugate for short. The coefficient of each term up to the tree level is determined by a diagrammatic calculation, as discussed in detail in Appendix A.

To mimic the junction structure close to the interface at $z = 0$, the following conditions are set:

$$\begin{aligned} \alpha_p(z) < 0, \quad \alpha_s(z) > 0, \quad &\text{for} \quad z > 0, \\ \alpha_p(z) > 0, \quad \alpha_s(z) < 0, \quad &\text{for} \quad z < 0, \end{aligned} \tag{5}$$

so that the $p_x + ip_y$ pairing dominates deep inside the upper space, whereas the s-wave pairing dominates deep inside the lower space. Due to the gradient terms led by K_p and K_s, the pairing gap function cannot exhibit a sudden change. Therefore, p_x-, p_y- and s-wave pairing symmetries should coexist close to the $z = 0$ interface.

To understand intuitively, we take a quick look at the phase-sensitive terms in the free energy. The phase sensitive g_{sp} and g_{pp} terms are

$$g_{sp}[\Delta_s^{*2}(\Delta_{p_x}^2 + \Delta_{p_y}^2) + \text{c.c.}] - g_{pp}|\Delta_{p_x}^* \Delta_{p_y} - \Delta_{p_y}^* \Delta_{p_x}|^2, \tag{6}$$

which can be evaluated as

$$2g_{sp}|\Delta_s|^2|\Delta_p|^2[\cos(2\phi_x - 2\phi_s) + \cos(2\phi_y - 2\phi_s)]$$
$$+ 2g_{pp}[\cos(2\phi_x - 2\phi_y) - 1], \tag{7}$$

where $\Delta_s = |\Delta_s|\exp(i\phi_s)$, $\Delta_{px} = |\Delta_p|\exp(i\phi_x)$, and $\Delta_{py} = |\Delta_p|\exp(i\phi_y)$. Each term in Eq. (7) is minimized if ϕ_x, ϕ_y, and ϕ_s mutually differ by $\pm\frac{\pi}{2}$. However, Eq. (7) is frustrated since a simultaneous mutual $\pm\frac{1}{2}\pi$ difference among three phases is impossible. Therefore, there will be competition among

the phases of the superconducting order parameters in the coexisting region.

To determine the pattern arising from the competition, we apply an iterative numerical method to obtain the solution of the pairing gap function by minimizing the free energy. The numerical results for the magnitudes and phases of the superconducting order parameters are displayed in Figs. 3(a) and 3(b), respectively. It is found that the solutions of the magnitudes $|\Delta_{p_x}|$ and $|\Delta_{p_y}|$ are equal, as shown in Fig. 3(a). As can be seen from Fig. 3(a), the system can be clearly divided into three regions: the region marked with I, where the s-wave pairing dominates (deep inside the s-wave bulk); region II between the two vertical dashed lines, where all three pairing symmetries coexist; and region III, where the p_x, p_y-wave pairings dominate (deep inside the bulk of the chiral p-wave superconductor). In the numerical calculations, the phase ϕ_s of the s-wave pairing is chosen to be zero for $z < 0$ and $|z/\xi_w| \gg 1$, where $\xi_w = \sqrt{|K_s/\alpha_s|}$ represents the width of the coexisting region. Then ϕ_s is solved to remain at zero in the entire junction, as indicated by the red line in Fig. 3(b).

As can be seen from Fig. 3(b), deep inside the p-wave bulk, Δ_{p_x} and Δ_{p_y} have a relative $\frac{\pi}{2}$ phase difference, and the magnitude of Δ_s is nearly negligible. When approaching the junction from the p-wave side, the magnitudes of Δ_{p_x} and Δ_{p_y} start shrinking, and so does the phase φ between them, whereas the magnitude of Δ_s keeps growing. Eventually, when leaving the coexisting region and entering the s-wave bulk, Δ_s is much larger than Δ_{px} and Δ_{py} in magnitude. We note that the three phases ϕ_x, ϕ_y, and ϕ_s exhibit the following pattern throughout the whole space:

$$\phi_x - \phi_y = \varphi,$$
$$\frac{\phi_x + \phi_y}{2} - \phi_s = \frac{\pi}{2}. \tag{8}$$

As a result, the tricomponent pairing gap function in the coexisting region can be written as $s + i[p_x \exp(i\varphi/2) + p_y \exp(-i\varphi/2)]$, as shown in Fig. 2(a), in which φ decreases from $\pi/2$ down to 0 as the junction is traversed from $z > 0$ to $z < 0$.

C. Symmetry-breaking pattern

In closing this section, we discuss the symmetry-breaking pattern in the junction region. Clearly, all symmetry transformations T, C_4, M_x, M_y, M_{x-y}, and M_{x+y} are spontaneously broken, where $M_{x,y}$ and $M_{x\pm y}$ represent the spin-orbit coupled reflection with respect to the x, y, and $x \pm y$ planes, respectively. Here, $L_z + \frac{1}{2}N$ is not conserved when $\beta'_p = 0$. However, the tricomponent pairing $s + i[p_x \exp(i\varphi/2) + p_y \exp(-i\varphi/2)]$ is invariant under TM_{x-y}. Hence, the unbroken symmetry group is $\langle TM_{x-y} \rangle \simeq \mathbb{Z}_2$, in which $\langle \cdots \rangle$ represents a group generated by the operations inside the bracket. As a result, the symmetry-breaking pattern for the tricomponent pairing is $C_{4v} \times \mathbb{Z}_2^T \to \mathbb{Z}_2$, in which $\mathbb{Z}_2^T$ on the left side of the arrow represents $\langle T \rangle$, i.e., the group generated by the time-reversal operation. Since $|C_{4v} \times \mathbb{Z}_2^T|/|\mathbb{Z}_2| = 8$, where $|...|$ represents the number of group elements, there are eight degenerate solutions of the pairing configurations
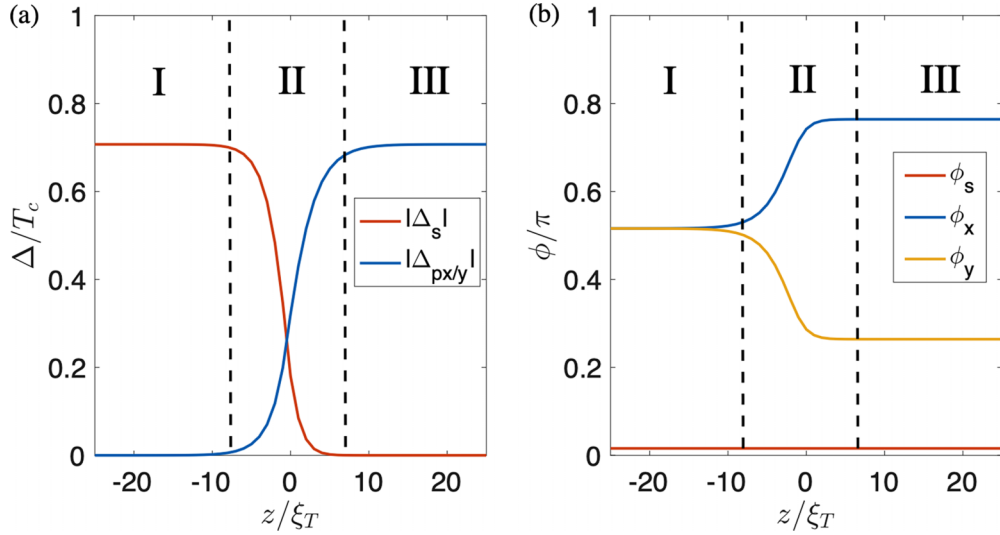
FIG. 3. (a) Magnitudes of the gap function $|\Delta_s|$ (red curve) and $|\Delta_{px}| = |\Delta_{py}|$ (blue curve) as functions of z and (b) their phases ϕ_s (red curve), ϕ_x (blue curve), and ϕ_y (yellow curve) as functions of z. The intervals of z marked by I, II, and III represent the regions where s-wave dominates, s- and p-wave coexist, and p-wave dominates, respectively. The units for $|\Delta_\lambda|$ ($\lambda = s, p_x, p_y$) and the spatial coordinate z are the transition temperature T_c and the coherence length $\xi_T = v_F/T_c$, respectively, where v_F is the Fermi velocity. The parameters in the numerical calculations are chosen as $K_s = K_p = 10N_F\xi_T^2$, $\alpha_s = 2\text{sgn}(z)N_F$, $\alpha_p = -\text{sgn}(z)N_F$, $\beta_s = 2N_F/T_c^2$, $\beta_p = 3.75N_F/T_c^2$, $\beta_p' = 0.5N_F/T_c^2$, $g_{sp} = 3.5N_F/T_c^2$, $g_{pp} = 3.5N_F/T_c^2$, and $\gamma = 10N_F/T_c^2$, where N_F is the density of states at the Fermi level, and T_c is the superconducting transition temperature.

given by

$$s + i\eta_1\left[\exp\left(\frac{i\eta_2\varphi}{2}\right)p_x + \eta_3\exp\left(-\frac{i\eta_2\varphi}{2}\right)p_y\right], \quad (9)$$

in which $\eta_j = \pm 1$ ($j = 1, 2, 3$).

On the other hand, the boundary condition deep in the p-wave bulk needs to be specified when minimizing the free energy, which amounts to fixing the chirality (i.e., $p_x + ip_y$ or $p_x - ip_y$) deep in the upper space. The choice of the boundary condition explicitly breaks the time-reversal and reflection symmetries since they both flip the chirality. By putting the s- and chiral p-wave superconducting layers in contact with each other, the junction structure further breaks the residual C_4 symmetry [83], where the action of the C_4 rotational operation on the chiral p-wave pairing is defined up to a gauge transformation. The corresponding four degenerate tricomponent pairing configurations among the eight in Eq. (9) satisfy $\eta_2\eta_3 = -\eta_c$, when the boundary condition is chosen as $p_x + i\eta_c p_y$, where $\eta_c = \pm 1$. Figures 2(a)–2(d) display the configurations for the positive chirality case (i.e., $p_x + ip_y$), and the other four negative chirality configurations can be obtained from those in Fig. 2 by switching Δ_{px} and Δ_{py}.

Finally, we note that, although the analysis is performed in the framework of GL free energy, which can only be derived from the BCS theory in the vicinity of the superconducting transition temperatures, one may question the validity of the GL analysis since the transition temperatures of s- and p-wave superconductors could mismatch. Nevertheless, the GL formalism can be viewed as the complex ϕ_4 theory based on symmetry properties on a general basis. The coefficients of α_p in Eq. (1) and α_s in Eq. (4) become nonanalytic when temperatures are far below T_c. Our analysis below does not depend on the details of the quadratic terms but on the quartic terms f_{sp} and f_{pp} which remain regular even far below T_c.

Hence, the obtained symmetry-breaking pattern and the pairing configurations in Eq. (9) are robust to junction details and the temperature range. Therefore, the characteristic features of the tricomponent pairing equally applies deep in the ordered phase, extending beyond the applicable range of the GL free-energy analysis.

III. ANISOTROPIC MAGNETOELECTRIC EFFECT AND EDGE MAGNETIZATION

In this section, we discuss a type of anisotropic magnetoelectric effect in the tricomponent pairing heterojunction. Using a linear response approach, we show that a spatial variation of the electric potential can induce spin magnetizations along the z direction with a strength dependent on the direction of the electric field. Since an edge corresponds to a change of the electric potential, we conclude that the edge of the heterojunction carries anisotropic spin magnetization if the potential change in the vicinity of the edge is slow enough such that the linear response approximation applies. In the next section, we make a complimentary analysis on the opposite limit where the electric potential changes abruptly at the edge. The anisotropic edge magnetization is shown to emerge as the consequence of the splitting between the two branches of chiral Majorana edge modes. Therefore, the soft and hard edge pictures on the edge magnetization are fully consistent with each other.

Before proceeding, we first note that there is no spin magnetization along the z direction for a uniform system. This can be directly seen by noticing that, in the tricomponent pairing $s + i\eta_1[\exp(i\eta_2\varphi/2)p_x + \eta_3\exp(-i\eta_2\varphi/2)p_y]$, the Cooper pairings always occur between up and down electrons, thereby carrying no spin-angular momentum S^z.
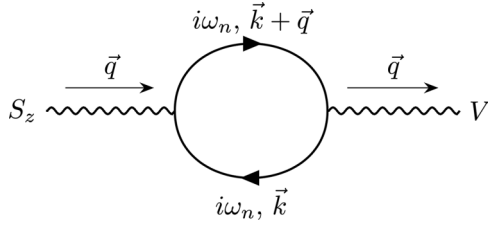
FIG. 4. The Feynman diagram for the response of the spin magnetization S^z to an external static electric potential V.

Next, we study the induced magnetization in the presence of a spatially varying electrical potential. In the linear response theory, this is captured by the response of the spin-magnetization density $S^z(\vec{r})$ to an applied electric potential $V(\vec{r})$, as shown by the bubble diagram in Fig. 4. Assuming $V(\vec{r})$ to be slowly varying, we will only calculate the results up to linear order in the wave vector $\vec{q}$. The solid lines in Fig. 4 represent the fermionic Green's functions $G(i\omega_n, \vec{k})$ in the superconducting state, where $\omega_n = (2n+1)\pi T$ ($n \in \mathbb{Z}$) is the fermionic Matsubara frequency, and the dashed lines are the bosonic field $S^z(\vec{r})$ or $V(\vec{r})$. In the following, we assume that $\vec{r}$ represents the two-dimensional (2D) spatial coordinates within the junction interface.

In the momentum space within the Bogoliubov–de Gennes (BdG) formalism, the pairing $\hat{\Delta}(\vec{k})$, the spin density $\hat{S}_z(\vec{q})$, and the particle number density $\hat{\rho}(\vec{q})$ can be represented as

$$\hat{S}^z(\vec{q}) = \psi^\dagger(\vec{k}+\vec{q})S^z(\vec{q})\psi(\vec{k}),$$
$$\hat{\rho}^x(\vec{q}) = \psi^\dagger(\vec{k}+\vec{q})\rho(\vec{q})\psi(\vec{k}),$$
$$\hat{\Delta}(\vec{k}) = \psi^\dagger(\vec{k})\Delta(\vec{k})\psi^{\dagger,T}(\vec{k}), \tag{10}$$

in which $\psi(\vec{k}) = [c_\uparrow(\vec{k}), c_\downarrow(\vec{k}), c_\uparrow^\dagger(-\vec{k}), c_\downarrow^\dagger(-\vec{k})]^T$, and the 4×4 matrix kernels are

$$S^z(\vec{q}) = \frac{1}{4}\sigma^z\tau^z, \quad \rho(\vec{q}) = \frac{1}{2}\tau^z,$$

$$\Delta(\vec{k}) = -|\Delta_s|\sigma^y\tau^y - \frac{|\Delta_p|}{k_f}$$

$$\times \left[(k_x + k_y)\sigma^x\tau^y \cos\frac{\varphi}{2} + (k_x - k_y)\sigma^x\tau^x \sin\frac{\varphi}{2}\right], \tag{11}$$

in which τ^j ($j = x, y, z$) are the Pauli matrices in the Nambu space, and the tricomponent structure $s + i[\exp(i\frac{\varphi}{2})p_x + \exp(-i\frac{\varphi}{2})p_y]$ is assumed. For simplicity, we take a rotationally invariant band dispersion $\xi(\vec{k}) = \frac{\hbar^2}{2m}(k^2 - k_f^2)$. Using the Green's function:

$$G(i\omega_n, \vec{k}) = \frac{1}{i\omega_n - \xi(\vec{k})\tau^z - \Delta(\vec{k})}, \tag{12}$$

the diagram in Fig. 4 can be evaluated as

$$\chi(\vec{q}) = -\int \frac{d^2k}{(2\pi)^2} \frac{1}{\beta}$$
$$\times \sum_{i\omega_n} \text{Tr}[S_z G(i\omega_n, \vec{k}+\vec{q}) V G(i\omega_n, \vec{k})]$$
$$= \chi_0(iq_x + iq_y), \tag{13}$$

in which, within the limit $|\Delta_s|, |\Delta_p| \ll T$ (i.e., close to the superconducting transition temperature), χ_0 is calculated to be

$$\chi_0 \approx \frac{7\zeta(3)}{8\sqrt{2}\pi^2} N_F \frac{1}{T^2} \frac{|\Delta_p\Delta_s|}{k_f} \cos\frac{\varphi}{2}, \tag{14}$$

where ζ, N_F, and T are the Riemann zeta function, the density of states at Fermi level, and the temperature, respectively. In Eq. (13), the $\vec{q}$-independent terms vanish, and only the terms linear in $\vec{q}$ are kept. Detailed calculations are included in Appendix B.

The form of $\chi(\vec{q})$ in Eq. (13) implies the following response relation in real space:

$$S^z(\vec{r}) = \chi_0(\partial_x V + \partial_y V) = \sqrt{2}\chi_0 \hat{n}_0 \cdot \nabla V, \tag{15}$$

in which $\hat{n}_0 = \frac{1}{\sqrt{2}}(1, 1, 0)$. As is clear from Eq. (15), the response is anisotropic since there is a special direction $\hat{n}_0$, which is simply a consequence of the breaking of the C_4 symmetry. Also notice that the two sides of Eq. (15) are both invariant under the unbroken symmetry transformation TM_{x-y}. Indeed, the invariance under TM_{x-y} can completely determine $\hat{n}_0$ to be parallel with the (110) direction. We emphasize that, although the response in Eq. (15) is obtained by simplifying the junction region as a 2D problem, Eq. (15) equally applies in the more rigorous three-dimensional (3D) treatment by considering the averaged response over the z direction, as proved in Appendix C based on a symmetry analysis, except that the susceptibility χ_0 will have a renormalized value.

Finally, we note that the edge can be modeled by a change of the electric potential. The potential in the vacuum side is higher than the Fermi energy in the bulk so that the electrons in the vacuum are completely depleted. Consider a soft edge where the electric potential varies slowly. Since $\nabla V = |\vec{\nabla}V|(\cos\theta, \sin\theta, 0)$ is parallel to the normal direction of the edge, it is clear from Eq. (15) that a spin magnetization emerges on the edge. For a rough estimation, $|\vec{\nabla}V|$ can be approximated as $\sim \epsilon_f/\xi_c$, where $\epsilon_f = \frac{\hbar^2}{2m}k_f^2$ is the Fermi energy and ξ_c is the coherence length. Therefore, the edge magnetization along the z axis can be estimated as

$$S_z(\theta) \sim \sqrt{2}\chi_0 \frac{\epsilon_f}{\xi_c}(\cos\theta + \sin\theta), \tag{16}$$

which is highly dependent on the normal direction of the edge. Assuming the edge to be in a circular shape, the edge magnetization along the z direction is illustrated in Fig. 5, where the height of the red arrows indicates the strength of the spin polarizations.

IV. EDGE STATE PICTURE OF THE EDGE MAGNETIZATION

In this section, we consider a hard edge which is assumed to be an infinite straight line. The system lies on one side of the edge, and the other side is the vacuum. The boundary condition is taken such that the wave function vanishes at the edge and in the vacuum. We show that the edge magnetization discussed in Sec. III with a soft edge can alternatively be understood in the edge-state picture.
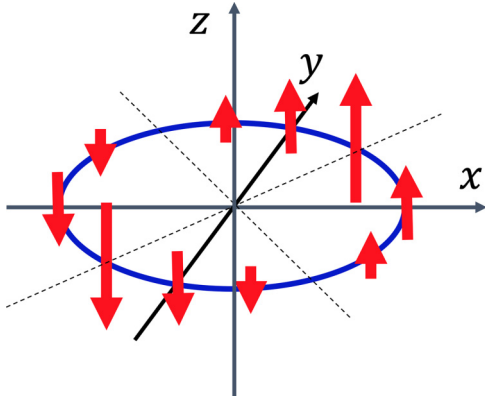
FIG. 5. The anisotropic edge magnetization on a circular boundary of the junction. The edge is represented by the blue circle. The direction and magnitude of the edge magnetization are represented by the direction and height of the red arrows, respectively.

For simplification of discussion, we perform a rotation of the coordinate system defined as

$$\begin{pmatrix} x \\ y \end{pmatrix} = \begin{pmatrix} \cos\theta & -\sin\theta \\ \sin\theta & \cos\theta \end{pmatrix} \begin{pmatrix} x' \\ y' \end{pmatrix}. \quad (17)$$

In the rotated basis, $\hat{x}'$ is along the normal direction $\hat{n} = \hat{x}\cos\theta + \hat{y}\sin\theta$ of the edge, and k_y' is a good quantum number. After the rotation, the superconducting pairing gap function is transformed into

$$\hat{\Delta}' = \frac{1}{k_f}[\Delta_{px}'(-i\partial_x') + \Delta_{py}'k_y']\sigma^z i\sigma^y + \Delta_s i\sigma^y, \quad (18)$$

in which

$$\Delta_{pv}' = |\Delta_p|\left[(\cos\theta + \sin\theta)\cos\frac{\varphi}{2}\right.$$
$$\left. + \epsilon(v)i(\cos\theta - \sin\theta)\sin\frac{\varphi}{2}\right], \quad (19)$$

where $v = x, y$, and $-\epsilon(x) = \epsilon(y) = 1$. To further simplify the problem, a gauge transformation can be performed to absorb the phase of Δ_{px}'. Then the pairing acquires the form:

$$\hat{\Delta}'' = \frac{1}{k_f}[\Delta_{px}''(-i\partial_x') + \Delta_{py}''k_y']\sigma^z i\sigma^y + \Delta_s'' i\sigma^y, \quad (20)$$

in which

$$\Delta_{px}'' = |\Delta_p|\sqrt{1 + \sin(2\theta)\cos\varphi},$$
$$\Delta_{py}'' = |\Delta_p|\frac{\cos(2\theta)\cos\varphi + i\sin\varphi}{\sqrt{1 + \sin(2\theta)\cos\varphi}},$$
$$\Delta_s'' = i\Delta_s\frac{\cos\frac{\varphi}{2}(\cos\theta + \sin\theta) + i\sin\frac{\varphi}{2}(\cos\theta - \sin\theta)}{\sqrt{1 + \sin(2\theta)\cos\varphi}}.$$
$$(21)$$

In what follows, we assume that the junction occupies the $x' < 0$ region, whereas $x' > 0$ is the vacuum. The boundary condition is taken such that the wave function vanishes when $x' \geqslant 0$.

The general solutions of the edge states are rather complicated. To illustrate the essential physics, it is enough to
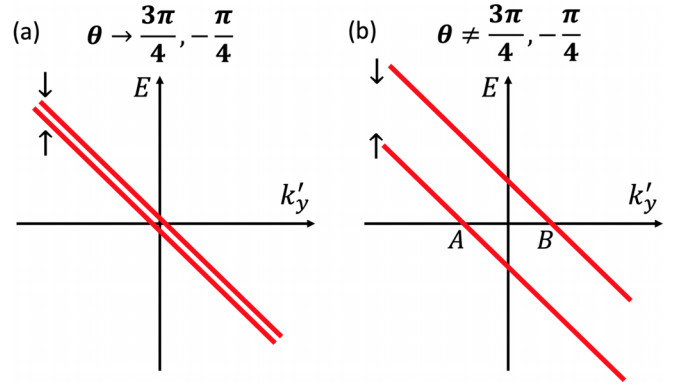

FIG. 6. Dispersions of the chiral edge Majorana modes for (a) $\theta = \frac{3\pi}{4}, -\frac{\pi}{4}$ and (b) $\theta \neq \frac{3\pi}{4}, -\frac{\pi}{4}$, where $\theta \in [-\pi, \pi]$.

consider the limit $|\Delta_s| \ll |\Delta_p|$. The strategy is first solving the edge states for $k_y' = 0$, and then a nonzero k_y' can be included using a $k \cdot p$ perturbation method. In the absence of the s-wave component, there are two Majorana zero modes localized around the boundary for $k_y' = 0$. In the weak pairing limit $|\Delta_p| \ll \epsilon_f$, the wave functions of the two zero modes can be solved as [61]

$$\Phi_\uparrow(x') = \left[\exp\left(-i\frac{\pi}{4}\right), 0, 0, \exp\left(i\frac{\pi}{4}\right)\right]^T u(x),$$
$$\Phi_\downarrow(x') = \left[0, \exp\left(-i\frac{\pi}{4}\right), \exp\left(i\frac{\pi}{4}\right), 0\right]^T u(x), \quad (22)$$

in which $u(x) = \frac{1}{\sqrt{N}}\sin(k_f x)\exp(\frac{m|\Delta_p|}{\hbar k_f}x)$, where N is a normalization factor. Since $|\Delta_s| \ll |\Delta_p|$, the s-wave pairing can be treated using a first-order perturbation. It is straightforward to verify that the projection of $\hat{\Delta}_s$ [defined in Eq. (2)] to the basis $\{\Phi_\uparrow, \Phi_\downarrow\}$ is $-(\text{Im}\Delta_s'')s^z$, where s^α ($\alpha = x, y, z$) are the Pauli matrices in the space spanned by $\{\Phi_\uparrow, \Phi_\downarrow\}$, and $\text{Im}\Delta_s''$ can be read from Eq. (21). Therefore, while the Majorana modes remain at zero energy under the real part of Δ_s'', the imaginary part of Δ_s'' opens a gap on the edge.

Next, we move to a nonzero k_y'. The $k \cdot p$ Hamiltonian can be obtained by projecting the pairing along the y' direction to the basis $\{\Phi_\uparrow, \Phi_\downarrow\}$, and the result is $-\frac{\text{Im}\Delta_{py}''}{k_f}k_y's^0$, where s^0 is the 2×2 identity matrix. Combining with the contribution from the $\text{Im}\Delta_s''$ term, the dispersions of the two chiral Majorana edge fermions can be derived as

$$E_\eta(k_y') = -\frac{\text{Im}\Delta_{py}''}{k_f}k_y' - \eta\text{Im}\Delta_s'', \quad (23)$$

in which $E_\eta(k_y')$ is the dispersion of the η branch of the chiral modes, where $\eta = 1$ (-1) for $\uparrow$ $(\downarrow)$. Therefore, when an s-wave component is present in the pairing, the two edge modes split by an energy gap $\Delta E = 2\text{Im}\Delta_s''$. Since $\text{Im}\Delta_s''$ vanishes when $\theta = 3\pi/4, -\pi/4$, the spin-up and down chiral branches coincide with each other, as shown in Fig. 6. When $\theta \neq 3\pi/4, -\pi/4$, the two branches split due to the opening of the gap, as shown in Fig. 6(b).

The two branches of chiral Majorana edge modes are spin polarized. As can be seen from Eq. (23), within the approximation of a linear dispersion, the occupation range of k_y' for
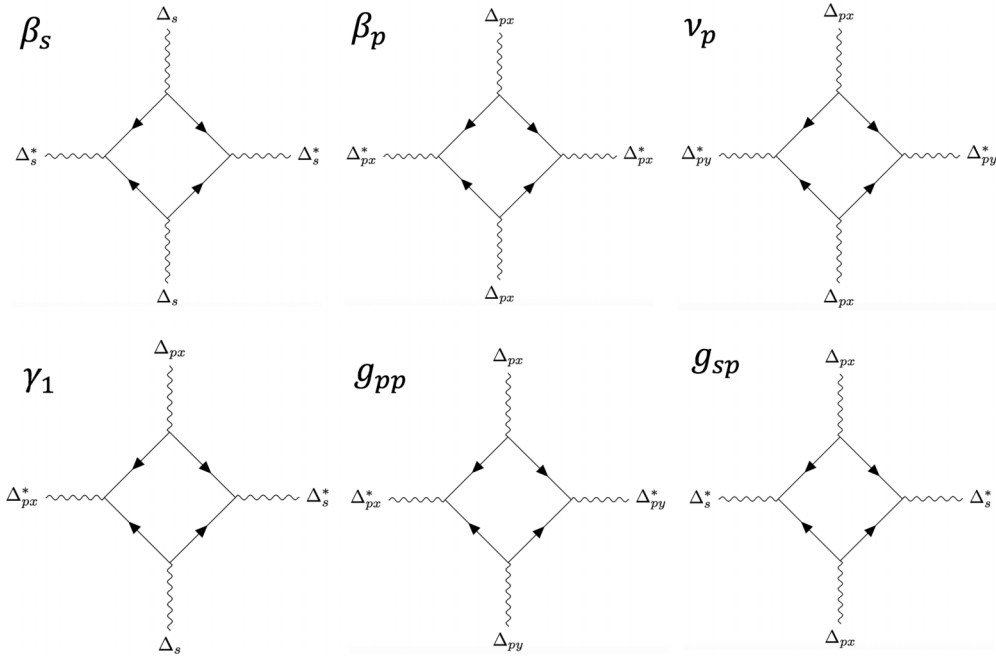
FIG. 7. Diagrams determining the coefficients in the Ginzburg-Landau free energy.

the λ branch of the chiral mode is $\epsilon_\lambda \frac{\text{Im}\Delta_s''}{\text{Im}\Delta_{py}''} k_f \leqslant k_y' \leqslant k_f$, in which $\epsilon_\lambda = 1$ (-1) for $\lambda = \uparrow$ ($\downarrow$). This leads to an imbalance in the occupation range between the up and down chiral edge modes corresponding to the line segment between points A and B in Fig. 6(b). As a consequence, a spin polarization develops on the edge, which has a direction dependence proportional to $\text{Im}\Delta_s''/\text{Im}\Delta_y'' \sim (\sin\theta + \cos\theta)$. This result is consistent with what has been obtained in Sec. III, as shown in Fig. 5. Thus, we see that the soft and hard edge pictures on the edge magnetization are fully consistent with each other.

Finally, we also note that experiments on the anisotropic effect of the edge magnetization in the heterojunction could be potentially useful for testing the gap function symmetries of unconventional superconductors.

V. CONCLUSIONS

In conclusion, we have studied the heterojunction with one side possessing the chiral p-wave (i.e., $p_x \pm ip_y$) and the other side the conventional s-wave pairing gap functions. By employing a GL free-energy analysis, the pairing gap function in the junction region is shown to exhibit a frustrated tricomponent structure as $s + i\eta_1[\exp(i\eta_2\varphi/2)p_x + \eta_3 \exp(-i\eta_2\varphi/2)p_y]$, where φ is the phase difference between the p_x and p_y components, and $\eta_j = \pm1$ ($j = 1, 2, 3$). By solving the chiral Majorana edge modes with the tricomponent pairing, we find that the edge of the junction carries an anisotropic spin magnetization, where the anisotropy originates from the breaking of the rotational symmetry. In addition, the edge magnetization is consistent with a type of anisotropic magnetoelectric effect, which is analyzed through the linear response calculation.

APPENDIX A: THE GL FREE ENERGY

For simplicity, we will consider a system with isotropic Fermi surface. As a result, the β_p' term vanishes. Only keeping the spatially uniform parts, the free energy up to quartic orders is

$$f_{spp} = \alpha_s|\Delta_s|^2 + \alpha_p(|\Delta_{px}|^2 + |\Delta_{py}|^2) + \beta_s|\Delta_s|^4 + \beta_p(|\Delta_{px}|^4 + |\Delta_{py}|^4) + g_{pp}[(\Delta_{px}^*\Delta_{py})^2 + (\Delta_{py}^*\Delta_{px})^2]$$

$$+ v_p|\Delta_{px}|^2|\Delta_{py}|^2 + \gamma_1(|\Delta_{px}|^2 + |\Delta_{py}|^2)|\Delta_s|^2 + g_{sp}[\Delta_s^{*2}(\Delta_{px}^2 + \Delta_{py}^2) + \Delta_s^2(\Delta_{px}^{*2} + \Delta_{py}^{*2})]. \tag{A1}$$

While the coefficients of the quadratic terms depend on the interactions which rely on the details of the pairing mechanism, the coefficients of the quartic terms are not dependent on the interaction strength within a tree-level approximation and can be

determined from the diagrams in Fig. 7, in which the the superconducting order parameters are given by

$$\hat{\Delta}_s = \frac{\Delta_s}{2} \sum_k c_k^\dagger i\sigma^y (c_{-k}^\dagger)^T, \quad \hat{\Delta}_{px} = \frac{\Delta_{px}}{2k_f} \sum_k c_k^\dagger (k_x \sigma^z) i\sigma^y (c_{-k}^\dagger)^T, \quad \hat{\Delta}_{py} = \frac{\Delta_{py}}{2k_f} \sum_k c_k^\dagger (k_y \sigma^z) i\sigma^y (c_{-k}^\dagger)^T, \tag{A2}$$

where $c_k^\dagger = (c_{k\uparrow}^\dagger \ c_{k\downarrow}^\dagger)$ is a two-component row vector.

Keeping only the static and uniform terms (i.e., zero frequency and zero momentum), we obtain

$$\beta_s = \frac{3}{2}\hat{\beta}_0 \text{Tr}\{(i\sigma^y)^\dagger (i\sigma^y)(i\sigma^y)^\dagger (i\sigma^y)\},$$

$$\beta_p = \frac{3}{2}\hat{\beta}_0 \frac{1}{k_f^4} \text{Tr}\{(ik_\alpha\sigma^z\sigma^y)^\dagger (ik_\alpha\sigma^z\sigma^y)(ik_\alpha\sigma^z\sigma^y)^\dagger (ik_\alpha\sigma^z\sigma^y)\},$$

$$\nu_p = 6\hat{\beta}_0 \frac{1}{k_f^4} \text{Tr}\{(ik_x\sigma^z\sigma^y)^\dagger (ik_x\sigma^z\sigma^y)(ik_y\sigma^z\sigma^y)^\dagger (ik_y\sigma^z\sigma^y)\},$$

$$\gamma_1 = 6\hat{\beta}_0 \frac{1}{k_f^2} \text{Tr}\{(ik_\alpha\sigma^z\sigma^y)^\dagger (ik_\alpha\sigma^z\sigma^y)(i\sigma^y)^\dagger (i\sigma^y)\},$$

$$g_{pp} = \frac{3}{2}\hat{\beta}_0 \frac{1}{k_f^4} \text{Tr}\{(ik_x\sigma^z\sigma^y)^\dagger (ik_y\sigma^z\sigma^y)(ik_x\sigma^z\sigma^y)^\dagger (ik_y\sigma^z\sigma^y)\},$$

$$g_{sp} = 6\hat{\beta}_0 \frac{1}{k_f^2} \text{Tr}\{(i\sigma^y)^\dagger (ik_\alpha\sigma^z\sigma^y)(i\sigma^y)^\dagger (ik_\alpha\sigma^z\sigma^y)\}, \tag{A3}$$

in which k_α can be taken as either k_x or k_y, and the operation $\hat{\beta}_0$ acting on the expression to the right of it is defined as

$$\hat{\beta}_0[\cdots] = \frac{1}{\beta} \frac{1}{L^3} \sum_{\omega_m, k} \frac{1}{(\omega_m^2 + \xi_k^2)^2}[\cdots], \tag{A4}$$

where $\xi_k = \hbar^2 k^2/2m - \epsilon_F$, and L^3 is the volume of the system. In the weak pairing limit, a linearization of the dispersion can be performed. Changing the integration over $\vec{k}$ to spherical coordinates, we have

$$\hat{\beta}_0[\cdots] = N_F \frac{1}{\beta} \sum_n \int_{-\infty}^\infty d\epsilon \int_0^\pi \sin\theta d\theta \int_0^{2\pi} d\phi \frac{1}{\{[(2n+1)\pi/\beta]^2 + \epsilon^2\}^2}[\cdots], \tag{A5}$$

in which N_F is the density of states at the Fermi energy.

Plugging Eq. (A5) into Eq. (A3), performing the integrations, and summing over the Matsubara frequencies, we obtain

$$\beta_s = \tfrac{3}{2}\beta, \quad \beta_p = \tfrac{3}{10}\beta, \quad \nu_p = \tfrac{2}{5}\beta, \quad \gamma_1 = 2\beta, \quad g_{pp} = \tfrac{1}{10}\beta, \quad g_{sp} = 2\beta, \tag{A6}$$

in which

$$\beta = \frac{7\zeta(3)N_F}{8\pi^2 T^2}. \tag{A7}$$

Notice that, since $2(\beta_p - g_{pp}) = \nu_p$, the p-wave terms in Eq. (A1) can be recombined into the form in Eq. (1).

Finally, we note that the coefficients determined in this section are not accurate in real situations since there are notable renormalization effects, particularly when T is close to T_c.

APPENDIX B: THE LINEAR RESPONSE OF THE ANISOTROPIC MAGNETOELECTRIC EFFECT

We work in the ordered phase and calculate the correlation function between S^z and ρ. In the following calculations, we take the pairing as $-is + \exp(i\varphi/2)p_x + \exp(-i\varphi/2)p_y$. The pairing is taken as

$$\frac{\Delta_p}{k_f}\left[\exp\left(\frac{i\varphi}{2}\right)k_x + \exp\left(-\frac{i\varphi}{2}\right)k_y\right]\sigma^z i\sigma^y - i\Delta_s i\sigma^y$$

$$= \left\{ \begin{array}{cc} 0 & \frac{\Delta_p}{k_f}\cos\left(\frac{\varphi}{2}\right)(k_x+k_y) + i\left[\frac{\Delta_p}{k_f}\sin\left(\frac{\varphi}{2}\right)(k_x-k_y) - \Delta_s\right] \\ \frac{\Delta_p}{k_f}\cos\left(\frac{\varphi}{2}\right)(k_x+k_y) + i\left[\frac{\Delta_p}{k_f}\sin\left(\frac{\varphi}{2}\right)(k_x-k_y) + \Delta_s\right] & 0 \end{array} \right\}, \tag{B1}$$

in which both Δ_p and Δ_s are real and positive. In the spin-up sector, the BdG Hamiltonian is of the form:

$$
H_\uparrow(\vec{k}) = \left\{
\begin{array}{cc}
\xi(\vec{k}) & \frac{\Delta_p}{k_f}\cos\left(\frac{\varphi}{2}\right)(k_x+k_y)-i\left[\frac{\Delta_p}{k_f}\sin\left(\frac{\varphi}{2}\right)(-k_x+k_y)+\Delta_s\right] \\
\frac{\Delta_p}{k_f}\cos\left(\frac{\varphi}{2}\right)(k_x+k_y)+i\left[\frac{\Delta_p}{k_f}\sin\left(\frac{\varphi}{2}\right)(-k_x+k_y)+\Delta_s\right] & -\xi(-\vec{k})
\end{array}
\right\}
$$
$$
= \xi(\vec{k})\iota^z + \frac{\Delta_p}{k_f}\cos\left(\frac{\varphi}{2}\right)(k_x+k_y)\iota^x + \left[\frac{\Delta_p}{k_f}\sin\left(\frac{\varphi}{2}\right)(-k_x+k_y)+\Delta_s\right]\iota^y. \tag{B2}
$$

Since the spin-up and down sectors are related by a particle-hole transformation, it is enough to work in the spin-up sector. We also note that the matrix kernels for S^z and ρ in the spin-up sector are ι^z and $\frac{1}{2}\iota^0$, respectively, where ι^0 is the 2×2 identity matrix. In what follows, we write ι^α as σ^α ($\alpha = 0, x, y, z$) for simplicity.

In the imaginary time formalism, the diagram in Fig. 4 can be evaluated as

$$
\chi(\vec{q}) = -\int \frac{d^2\vec{k}}{(2\pi)^2}\frac{1}{\beta}\sum_{i\omega_n}\text{Tr}\left[\frac{1}{2}\sigma^0\frac{1}{i\omega_n-H_\uparrow(\vec{k}+\vec{q})}\sigma^3\frac{1}{i\Omega_n-H_\uparrow(\vec{k})}\right]
$$
$$
= -\int \frac{d^2\vec{k}}{(2\pi)^2}\frac{1}{\beta}\sum_{i\omega_n}\frac{1}{\omega_n^2+\xi^2(\vec{k}+\vec{q})+\frac{\Delta_p^2}{k_f^2}\cos^2\left(\frac{\varphi}{2}\right)(k_x+q_x+k_y+q_y)^2+\left[\frac{\Delta_p}{k_f}\sin\left(\frac{\varphi}{2}\right)(-k_x-q_x+k_y+q_y)+\Delta_s\right]^2}
$$
$$
\times\frac{1}{\omega_n^2+\xi^2(\vec{k})+\frac{\Delta_p^2}{k_f^2}\cos^2\left(\frac{\varphi}{2}\right)(k_x+k_y)^2+\left[\frac{\Delta_p}{k_f}\sin\left(\frac{\varphi}{2}\right)(-k_x+k_y)+\Delta_s\right]^2}
$$
$$
\times\text{Tr}\left(\frac{\sigma^0}{2}\left\{i\omega_n+\xi(\vec{k}+\vec{q})\sigma^z+\frac{\Delta_p}{k_f}\cos\left(\frac{\varphi}{2}\right)(k_x+q_x+k_y+q_y)\sigma^x+\left[\frac{\Delta_p}{k_f}\sin\left(\frac{\varphi}{2}\right)(-k_x-q_x+k_y+q_y)+\Delta_s\right]\sigma^y\right\}\right.
$$
$$
\left.\times\sigma^z\left\{i\omega_n+\xi(\vec{k})+\frac{\Delta_p}{k_f}\cos\left(\frac{\varphi}{2}\right)(k_x+k_y)\sigma^x+\left[\frac{\Delta_p}{k_f}\sin\left(\frac{\varphi}{2}\right)(-k_x+k_y)+\Delta_s\right]\sigma^y\right\}\right). \tag{B3}
$$

The trace term in Eq. (B3) can be evaluated to be

$$
\text{Tr}[\cdots] = -i\frac{\Delta_p}{k_f}\cos\left(\frac{\varphi}{2}\right)\left\{q_x\left[\frac{2\Delta_p}{k_f}\sin\left(\frac{\varphi}{2}\right)k_y+\Delta_s\right]+q_y\left[-\frac{2\Delta_p}{k_f}\sin\left(\frac{\varphi}{2}\right)k_x+\Delta_s\right]\right\}, \tag{B4}
$$

in which the linear-in-ω_n terms are neglected since they sum to zero after Matsubara frequency summation. Since the numerator of Eq. (B3) is already linear in $\vec{q}$, the $\vec{q}$'s in the denominator can be set to be zero since we only need the results up to $O(\vec{q})$. Then we arrive at

$$
\chi(\vec{q}) = iq_x\chi_x + iq_y\chi_y, \tag{B5}
$$

in which

$$
\chi_x = \frac{\Delta_p}{k_f}\cos\left(\frac{\varphi}{2}\right)\int\frac{d^2\vec{k}}{(2\pi)^2}\frac{1}{\beta}\sum_{i\omega_n}\frac{\frac{2\Delta_p}{k_f}\sin\left(\frac{\varphi}{2}\right)k_y+\Delta_s}{\omega_n^2+\xi^2(\vec{k})+\frac{\Delta_p^2}{k_f^2}\cos^2\left(\frac{\varphi}{2}\right)(k_x+k_y)^2+\left[\frac{\Delta_p}{k_f}\sin\left(\frac{\varphi}{2}\right)(-k_x+k_y)+\Delta_s\right]^2},
$$
$$
\chi_y = \frac{\Delta_p}{k_f}\cos\left(\frac{\varphi}{2}\right)\int\frac{d^2\vec{k}}{(2\pi)^2}\frac{1}{\beta}\sum_{i\omega_n}\frac{-\frac{2\Delta_p}{k_f}\sin\left(\frac{\varphi}{2}\right)k_x+\Delta_s}{\omega_n^2+\xi^2(\vec{k})+\frac{\Delta_p^2}{k_f^2}\cos^2\left(\frac{\varphi}{2}\right)(k_x+k_y)^2+\left[\frac{\Delta_p}{k_f}\sin\left(\frac{\varphi}{2}\right)(-k_x+k_y)+\Delta_s\right]^2}. \tag{B6}
$$

Next, to simplify the expressions of χ_x and χ_y, we perform a change of variable:

$$
k'_x = \frac{1}{\sqrt{2}}(k_x+k_y), \quad k'_y = \frac{1}{\sqrt{2}}(-k_x+k_y). \tag{B7}
$$

Then we have

$$
\chi_x = A_x + A_y + A_s, \quad \chi_y = -A_x + A_y + A_s, \tag{B8}
$$

in which

$$A_\alpha = \frac{\Delta_p}{k_f} \cos\left(\frac{\varphi}{2}\right) \int \frac{d^2\vec{k}'}{(2\pi)^2} \frac{1}{\beta} \sum_{i\omega_n} \frac{\frac{\sqrt{2}\Delta_p}{k_f} \sin\left(\frac{\varphi}{2}\right) k_\alpha'}{\omega_n^2 + \xi^2(\vec{k}') + \frac{2\Delta_p^2}{k_f^2} \cos^2\left(\frac{\varphi}{2}\right) k_x'^2 + \left[\frac{\sqrt{2}\Delta_p}{k_f} \sin\left(\frac{\varphi}{2}\right) k_y' + \Delta_s\right]^2},$$

$$A_s = \frac{\Delta_p}{k_f} \cos\left(\frac{\varphi}{2}\right) \int \frac{d^2\vec{k}'}{(2\pi)^2} \frac{1}{\beta} \sum_{i\omega_n} \frac{\Delta_s}{\omega_n^2 + \xi^2(\vec{k}') + \frac{2\Delta_p^2}{k_f^2} \cos^2\left(\frac{\varphi}{2}\right) k_x'^2 + \left[\frac{\sqrt{2}\Delta_p}{k_f} \sin\left(\frac{\varphi}{2}\right) k_y' + \Delta_s\right]^2}, \quad \text{(B9)}$$

in which $\alpha = x, y$. Clearly, A_α ($\alpha = x, y$) vanishes since the numerator is odd under the integration over $\int dk_\alpha'$.

In the limit $\Delta_s, \Delta_p \ll T$, the dependence on the order parameters in the denominators of A_s can be neglected, and we have

$$\chi_x = \chi_y \approx \frac{\Delta_p \Delta_s}{\sqrt{2} k_f} \cos\left(\frac{\varphi}{2}\right) \int \frac{d^2\vec{k}}{(2\pi)^2} \frac{1}{\beta} \sum_{i\omega_n} \frac{1}{\left[\omega_n^2 + \xi^2(\vec{k})\right]^2}. \quad \text{(B10)}$$

The integral can be evaluated as

$$\int \frac{d^2\vec{k}}{(2\pi)^2} \frac{1}{\beta} \sum_{i\omega_n} \frac{1}{\left[\omega_n^2 + \xi^2(\vec{k})\right]^2} = N_0 \frac{1}{\beta} \sum_{i\omega_n} \int d\epsilon \frac{1}{\left(\omega_n^2 + \epsilon^2\right)^2} = N_0 \frac{1}{\beta} \sum_{n\in\mathbb{Z}} \frac{\pi}{2} \frac{1}{|2\pi n/T|^3} = \frac{7\zeta(3)}{8\pi^2} N_0 \frac{1}{T^2}, \quad \text{(B11)}$$

in which ζ is the Riemann zeta function.

In summary, in the limit $\Delta_s, \Delta_p \ll T$, the response is

$$S^z = \chi_0 (\partial_x V + \partial_y V), \quad \text{(B12)}$$

in which

$$\chi_0 = \frac{7\zeta(3)}{8\sqrt{2}\pi^2} N_0 \frac{1}{T^2} \frac{\Delta_p \Delta_s}{k_f} \cos\left(\frac{\varphi}{2}\right). \quad \text{(B13)}$$

APPENDIX C: SYMMETRY CONSIDERATION OF EQ. (13)

In this Appendix, based on symmetry analysis, we show that the linear magnetoelectric response must be proportional to $\hat{n}_0 \cdot \nabla V$ in the full 3D treatment, consistent with Eq. (13).

We consider the averaged response of spin density over the z direction $\int dz S^z(\vec{r}_\parallel, z)$ in the presence of an electric potential $\varphi(\vec{r})$. In the framework of linear response, the averaged magnetoelectric response $\overline{\chi}$ with wave vector $\vec{q}_\parallel$ and frequency ω is determined by the following retarded response function:

$$\overline{\chi}(\vec{q}_\parallel; \omega) = \int_{-\infty}^{\infty} dt' d\vec{r}_\parallel' dz dz'$$
$$\times \exp[i\omega(t - t')] \exp[-i\vec{q}_\parallel \cdot (\vec{r}_\parallel - \vec{r}_\parallel')] \varphi(\vec{q}_\parallel, z')$$
$$\times \Theta(t - t') \langle G|[S^z(\vec{r}_\parallel, z; t), \rho(\vec{r}_\parallel', z'; t')]|G\rangle, \quad \text{(C1)}$$

in which $|G\rangle$ is the ground state of the 3D junction; Θ is the step function; $\varphi(\vec{q}_\parallel, z') = \int d\vec{r}_\parallel \exp(-i\vec{q}_\parallel \cdot \vec{r}_\parallel) \varphi(\vec{r}_\parallel, z')$ is the Fourier transformed electric potential in the xy plane; and translational symmetry of $|G\rangle$ in the xy plane is used. For simplicity, the zero temperature is considered, but the discussion is straightforwardly generalizable to finite temperatures.

Notice that the ground state is invariant under the unbroken symmetry operation TM_{x-y} (see the discussion of unbroken symmetry group in Sec. II C). Since spin operators are pseudovectors, the sign of S^z changes twice under M_{x-y} and T, and as a result, there is no sign flip in S^z under the combined operation TM_{x-y}. Using the following transformation properties:

$$TM_{x-y}: S^z(x, y, z; t) \rightarrow S^z(y, x, z; t), \quad \text{(C2)}$$

$$TM_{x-y}: \rho(x, y, z; t) \rightarrow \rho(y, x, z; t), \quad \text{(C3)}$$

we obtain

$$\overline{\chi}(q_x, q_y; \omega) = \overline{\chi}(q_y, q_x; \omega). \quad \text{(C4)}$$

For terms linear in q_x and q_y, Eq. (C4) excludes the $i(q_x - q_y)$ component and uniquely determines $\overline{\chi}$ to be proportional to $i(q_x + q_y)$. Notice that this feature is the same as Eq. (13) which is derived from a 2D calculation. Therefore, a 2D treatment of the junction region is enough to capture the qualitative features of the magnetoelectric response, although a full 3D calculation will in general give a renormalized value of the coefficient χ_0 in Eq. (13).

[1] C. Kallin and J. Berlinsky, Rep. Prog. Phys. **79**, 054502 (2016).

[2] N. Read and D. Green, Phys. Rev. B **61**, 10267 (2000).

[3] S. D. Sarma, C. Nayak, and S. Tewari, Phys. Rev. B **73**, 220502(R) (2006).

[4] L. Fu and C. L. Kane, Phys. Rev. Lett. **100**, 096407 (2008).

[5] J. D. Sau, R. M. Lutchyn, S. Tewari, and S. D. Sarma, Phys. Rev. Lett. **104**, 040502 (2010).

[6] J. C. Y. Teo and C. L. Kane, Phys. Rev. Lett. **104**, 046401 (2010).

[7] R. Yu, W. Zhang, H.-J. Zhang, S.-C. Zhang, X. Dai, and Z. Fang, Science **329**, 61 (2010).

[8] X.-L. Qi, T. L. Hughes, and S.-C. Zhang, Phys. Rev. B **82**, 184516 (2010).

[9] S. B. Chung, X.-L. Qi, J. Maciejko, and S.-C. Zhang, Phys. Rev. B **83**, 100512(R) (2011).

[10] A. Kitaev, Ann. Phys. **303**, 2 (2003).

[11] A. Kitaev, Ann. Phys. **321**, 2 (2006).

[12] M. Stone and S.-B. Chung, Phys. Rev. B **73**, 014505 (2006).

[13] J. Alicea, Y. Oreg, G. Refael, F. von Oppen, and M. P. A. Fisher, Nat. Phys. **7**, 412 (2011).

[14] B. I. Halperin, Y. Oreg, A. Stern, G. Refael, J. Alicea, and F. von Oppen, Phys. Rev. B **85**, 144501 (2012).

[15] A. P. Mackenzie and Y. Maeno, Rev. Mod. Phys. **75**, 657 (2003).

[16] Y. Maeno, S. Kittaka, T. Nomura, S. Yonezawa, and K. Ishida, J. Phys. Soc. Jpn. **81**, 011009 (2012).

[17] Y. Liu and Z.-Q. Mao, Physica C **514**, 339 (2015).

[18] Y. Maeno, H. Hashimoto, K. Yoshida, S. Nishizaki, T. Fujita, J. G. Bednorz, and F. Lichtenberg, Nature (London) **372**, 532 (1994).

[19] R. Joynt and L. Tallifer, Rev. Mod. Phys. **74**, 235 (2002).

[20] E. R. Schemm, W. J. Gannon, C. M. Wishne, W. P. Halperin, and A. Kapitulnik, Science **345**, 190 (2014).

[21] J. D. Strand, D. J. Van Harlingen, J. Kycia, and W. P. Halperin, Phys. Rev. Lett. **103**, 197002 (2009).

[22] K. E. Avers, W. J. Gannon, S. J. Kuhn, W. P. Halperin, J. A. Sauls, L. DeBeer-Schmitt, C. D. Dewhurst, J. Gavilano, G. Nagy, U. Gasser *et al.*, Nat. Phys. **16**, 531 (2020).

[23] C. Kallin and A. J. Berlinsky, J. Phys.: Condens. Matter **21**, 164210 (2009).

[24] C. Kallin, Rep. Prog. Phys. **75**, 042501 (2012).

[25] A. P. Mackenzie, T. Scaffidi, C. W. Hicks, and Y. Maeno, npj Quantum Mater. **2**, 40 (2017).

[26] K. Ishida, H. Mukuda, Y. Kitaoka, K. Asayama, Z. Q. Mao, Y. Mori, and Y. Maeno, Nature (London) **396**, 658 (1998).

[27] J. A. Duffy, S. M. Hayden, Y. Maeno, Z. Mao, J. Kulda, and G. J. McIntyre, Phys. Rev. Lett. **85**, 5412 (2000).

[28] F. Laube, G. Goll, H. v. Löhneysen, M. Fogelström, and F. Lichtenberg, Phys. Rev. Lett. **84**, 1595 (2000).

[29] A. P. Mackenzie, R. K. W. Haselwimmer, A. W. Tyler, G. G. Lonzarich, Y. Mori, S. Nishizaki, and Y. Maeno, Phys. Rev. Lett. **80**, 161 (1998).

[30] G. M. Luke, Y. Fudamoto, K. M. Kojima, M. I. Larkin, J. Merrin, B. Nachumi, Y. J. Uemura, Y. Maeno, Z. Q. Mao, Y. Mori *et al.*, Nature (London) **394**, 558 (1998).

[31] K. Nelson, Z. Mao, Y. Maeno, and Y. Liu, Science **306**, 1151 (2004).

[32] J. Xia, Y. Maeno, P. T. Beyersdorf, M. M. Fejer, and A. Kapitulnik, Phys. Rev. Lett. **97**, 167002 (2006).

[33] F. Kidwingira, J. Strand, D. Van Harlingen, and Y. Maeno, Science **314**, 1267 (2006).

[34] A. Pustogow, Y. Luo, A. Chronister, Y.-S. Su, D. A. Sokolov, F. Jerzembeck, A. P. Mackenzie, C. W. Hicks, N. Kikugawa, S. Raghu *et al.*, Nature (London) **574**, 72 (2019).

[35] G. Volovik, Phys. Lett. A **128**, 277 (1988).

[36] G. Volovik and V. Yakovenko, J. Phys.: Condens. Matter **1**, 5263 (1989).

[37] D. A. Ivanov, Phys. Rev. Lett. **86**, 268 (2001).

[38] N. B. Kopnin and M. M. Salomaa, Phys. Rev. B **44**, 9667 (1991).

[39] S. Tewari, S. D. Sarma, C. Nayak, C. Zhang, and P. Zoller, Phys. Rev. Lett. **98**, 010506 (2007).

[40] C. Zhang, S. Tewari, R. M. Lutchyn, and S. D. Sarma, Phys. Rev. Lett. **101**, 160401 (2008).

[41] M. Cheng, K. Sun, V. Galitski, and S. D. Sarma, Phys. Rev. B **81**, 024504 (2010).

[42] X.-L. Qi, T. L. Hughes, S. Raghu, and S.-C. Zhang, Phys. Rev. Lett. **102**, 187001 (2009).

[43] R. B. Laughlin, Phys. Rev. Lett. **80**, 5188 (1998).

[44] T. Senthil, J. B. Marston, and M. P. A. Fisher, Phys. Rev. B **60**, 4245 (1999).

[45] B. Horovitz and A. Golub, Phys. Rev. B **68**, 214503 (2003).

[46] Y. Jiang, D.-X. Yao, E. W. Carlson, H.-D. Chen, and J. P. Hu, Phys. Rev. B **77**, 235420 (2008).

[47] M. Sato, Y. Takahashi, and S. Fujimoto, Phys. Rev. B **82**, 134521 (2010).

[48] A. M. Black-Schaffer, Phys. Rev. Lett. **109**, 197001 (2012).

[49] R. Nandkishore, L. S. Levitov, and A. V. Chubukov, Nat. Phys. **8**, 158 (2012).

[50] W.-S. Wang, Y.-Y. Xiang, Q.-H. Wang, F. Wang, F. Yang, and D.-H. Lee, Phys. Rev. B **85**, 035414 (2012).

[51] M. L. Kiesel, C. Platt, W. Hanke, and R. Thomale, Phys. Rev. Lett. **111**, 097001 (2013).

[52] F. Liu, C.-C. Liu, K. Wu, F. Yang, and Y. Yao, Phys. Rev. Lett. **111**, 066804 (2013).

[53] A. M. Black-Schaffer and C. Honerkamp, J. Phys.: Condens. Matter **26**, 423201 (2014).

[54] C.-C. Liu, L.-D. Zhang, W.-Q. Chen, and F. Yang, Phys. Rev. Lett. **121**, 217001 (2018).

[55] D. M. Kennes, J. Lischner, and C. Karrasch, Phys. Rev. B **98**, 241407(R) (2018).

[56] Z. Yang, S. Qin, Q. Zhang, C. Fang, and J. Hu, Phys. Rev. B **98**, 104515 (2018).

[57] T. Huang, L. Zhang, and T. Ma, Sci. Bull. **64**, 310 (2019).

[58] C. Wu and J. E. Hirsch, Phys. Rev. B **81**, 020508(R) (2010).

[59] Y. Wang and A. Chubukov, Phys. Rev. B **90**, 035149 (2014).

[60] Y. Wang and L. Fu, Phys. Rev. Lett. **119**, 187003 (2017).

[61] W. Yang, C. Xu, and C. Wu, Phys. Rev. Res. **2**, 042047 (2020).

[62] W.-C. Lee, S.-C. Zhang, and C. Wu, Phys. Rev. Lett. **102**, 217002 (2009).

[63] L. H. Hu, P. D. Johnson, and C. Wu, Phys. Rev. Res. **2**, 022021(R) (2020).

[64] R. Thomale, C. Platt, W. Hanke, and B. A. Bernevig, Phys. Rev. Lett. **106**, 187003 (2011).

[65] C. Platt, R. Thomale, C. Honerkamp, S.-C. Zhang, and W. Hanke, Phys. Rev. B **85**, 180502(R) (2012).

[66] M. Khodas and A. V. Chubukov, Phys. Rev. Lett. **108**, 247003 (2012).

[67] R. M. Fernandes and A. J. Millis, Phys. Rev. Lett. **111**, 127001 (2013).

[68] A. Hinojosa, R. M. Fernandes, and A. V. Chubukov, Phys. Rev. Lett. **113**, 167001 (2014).

[69] S.-Z. Lin, S. Maiti, and A. Chubukov, Phys. Rev. B **94**, 064519 (2016).

[70] V. Stanev and Z. Tešanović, Phys. Rev. B **81**, 134522 (2010).

[71] S.-Z. Lin and X. Hu, Phys. Rev. Lett. **108**, 177005 (2012).

[72] M. Marciani, L. Fanfarillo, C. Castellani, and L. Benfatto, Phys. Rev. B **88**, 214508 (2013).

[73] S. Maiti and A. V. Chubukov, Phys. Rev. B **87**, 144511 (2013).

[74] F. Ahn, I. Eremin, J. Knolle, V. B. Zabolotnyy, S. V. Borisenko, B. Büchner, and A. V. Chubukov, Phys. Rev. B **89**, 144513 (2014).

[75] J. Garaud and E. Babaev, Phys. Rev. Lett. **112**, 017003 (2014).

[76] S. Maiti, M. Sigrist, and A. Chubukov, Phys. Rev. B **91**, 161102(R) (2015).

[77] J. Garaud, J. Carlström, and E. Babaev, Phys. Rev. Lett. **107**, 197001 (2011).

[78] J. Garaud, Johan Carlström, E. Babaev, and M. Speight, Phys. Rev. B **87**, 014507 (2013).

[79] S.-Z. Lin, J. Phys.: Condens. Matter **26**, 493202 (2014).

[80] Y. S. Yerin and A. N. Omelyanchouk, Low Temp. Phys. **40**, 943 (2014).

[81] Y. Yerin, A. Omelyanchouk, S.-L. Drechsler, D. V. Efremov, and J. van den Brink, Phys. Rev. B **96**, 144513 (2017).

[82] A. J. Leggett, *Quantum Liquids: Bose Condensation and Cooper Pairing in Condensed-Matter Systems* (Oxford University Press, New York, 2006).

[83] Here, we note that, strictly speaking, the residual symmetry group is not just C_4. The full residual symmetries of the $p_x + ip_y$ pairing are $\{1, r, r^2, r^3, TM_x, G'TM_y, GTM_{x-y}, G^{-1}TM_{x+y}\}$, which is isomorphic to C_{4v}, where $r = GR(\hat{z}, \pi/2)$; $M_{f(x,y)}$ represents the spin-orbit coupled reflection with respect to the $f(x, y) = 0$ plane; G is the gauge transformation by $\pi/4$; and G' is the gauge transformation by $\pi/2$. If we remove the time-reversal operation, then the symmetry group becomes C_4.